EVLA Memo 103
Performance Tests of the EVLA K- and Q-Band Systems

Rick Perley, Bob Hayward, Bryan Butler, Vivek Dhawan
NRAO

March 1, 2006

Abstract

Sensitivity measurements performed on EVLA antenna #14 show that the cold-sky zenith system temperature is about 45K for the 18 – 26 GHz band, and 60 K for the low frequency end of the 40 – 50 GHz band, rising to 95 K at the high frequency end. Efficiency measurements based on the planet Venus show the antenna efficiency to be about 50% in the 18 – 26 GHz band, and about 28% for the 40 – 50 GHz band. The 18 – 26 GHz band performance easily meets EVLA requirements. The 40 – 50 GHz band requirements are met for system temperature, but the observed efficiency falls short of the required value of 34%. We expect to meet this requirement after implementation of better focusing, pointing, and a final round of holography.

1 Introduction

A primary requirement for the EVLA is to provide complete frequency coverage from 1 to 50 GHz with the highest possible sensitivity. This requirement will be met by installation of eight high-performance wide-bandwidth cryogenically-cooled receivers and feeds, two of which are the 18 – 26.5 GHz (K-band) and 40 – 50 GHz (Q-band) systems. For both bands, the receivers and feeds are upgraded versions of the existing VLA systems.

We report here on the results of performance tests on the K and Q-band receivers systems mounted in EVLA antenna #14. The parameters measured were: receiver temperature, cold-sky system temperature, noise diode temperature, ground spillover temperature, optimum subreflector position (focus and rotation), and the characteristics of the atmospheric emission. All were determined at three frequencies within each band, chosen to span the full RF tuning range.

2 Test Setup and Observations

The purpose of these measurements was to ascertain the performance of the EVLA's K- and Q-band antenna/feed/receiver systems. To avoid any degradation due to the IF and digital transmission systems, it is advantageous to make the measurements as early in the signal transmission path as convenient, using total power rather than interferometric methods. For these tests, the power was measured at the output of the T303 module (the 'UX Downconverter'), using the same total power measurement system employed for the L-Band and C-band tests, as described in EVLA Memos #85 and #90. Although the effects of the T303 module are thus included, we utilized its so-called 'straight-through' path, thus avoiding a second downconversion. All measurements were made with 100 MHz BW at an IF frequency of 11000 MHz for the K-band measurements, and 8400 MHz for the Q-band measurements. The setup is shown in schematic form in Fig. 1.

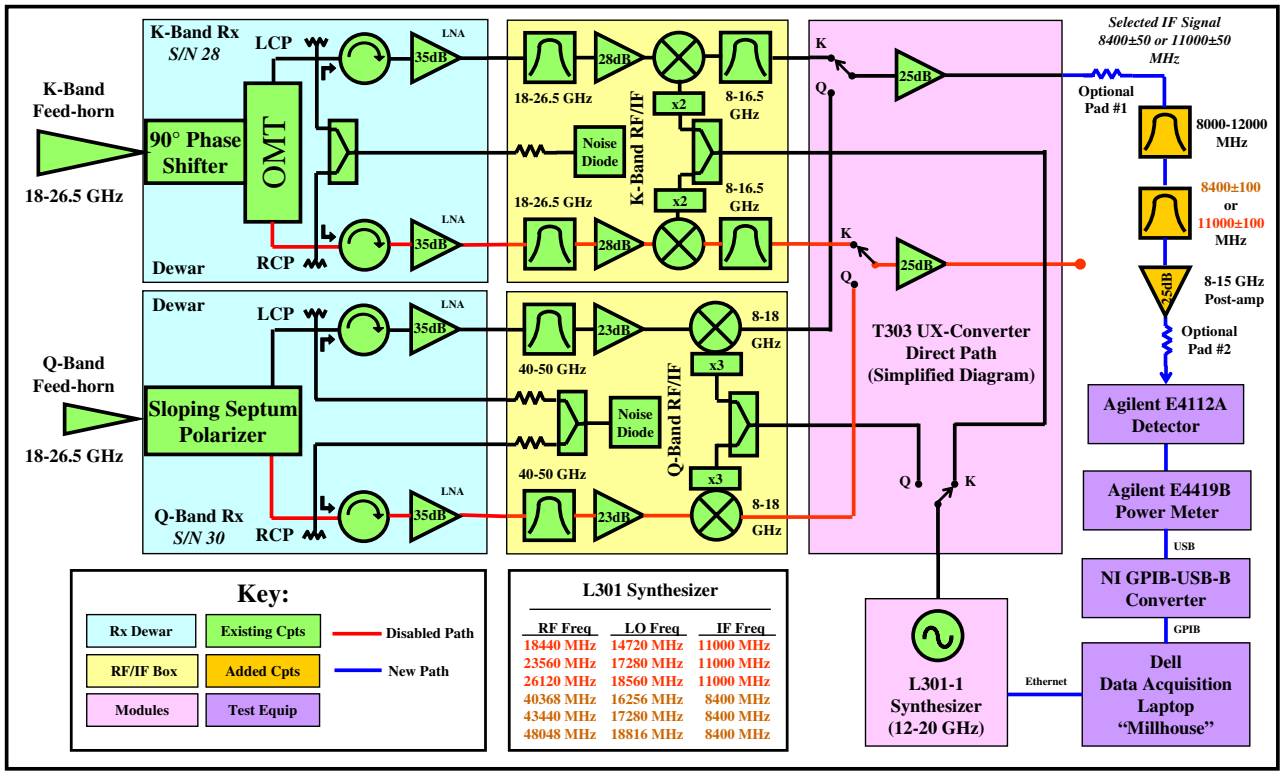

Figure 1: The setup used for determining the performance of the K and Q band receivers. The RF signals from the dewers (blue boxes) are downcoverted at the receiver (yellow boxes) and selected within the T303 UX Converter (pink box), which was configured to its 'straight through' signal path. The output IF signal was bandpass limited by filters (gold boxes), and the power levels set by use of pads and post-amplifiers to a cold-sky level of approximately −35dBm required for a linear response by the power meter over the power range from the cold sky to the hot loads (maximum range of 10 dB). The power measuring system (purple boxes) comprised an Agilent E4112A detector and E4419B power meter, whose data were recorded on a Dell Laptop (a.k.a. 'Millhouse'), using a Labview data acquisition program.

The observations used to determine system temperatures, spillover, and atmospheric characteristics were taken on 29 June, 2005 at three frequencies within each band: 18440, 23560, and 26120 MHz within K-band, and 40368, 43440 and 48048 MHz within Q-band. These frequencies were chosen to span nearly the full tuning range of each receiver. The weather conditions were excellent for observations at these frequencies – clear and calm with air temperature near 30C, and dew point near 12C.

The data used to determine the antenna efficiency, optimum subreflector positioning, and antenna beam shape were taken on (TBD), at the same frequencies.

3 Methodology

Determination of the system temperature, receiver temperature, spillover temperature, and atmospheric emission utilized the same 'hot-cold' load method described in EVLA Memos #85 and 90.

The hot load consisted of a piece of absorber large enough to cover the horn aperture. Two different absorbers were utilized – a white-jacketed thick absorber of unknown material whose temperature was monitored with an inserted thermometer, and a piece of Eccosorb CV-3, designed

for millimeter-wave applications. This absorber is black, much thinner (7.5 cm), and without a thermometer. Earlier tests had clearly shown that these two absorbers provided slightly different power input, due either to differing temperature, or to different absorber opacities. To separate these effects, we utilized these absorbers in different combinations. The results are given in the Appendix.

In our earlier L- and C-band measurements, the size of the horn apertures prevented use of a proper, liquid-nitrogen-cooled cold load, and we had to use the cold sky instead, introducing a small but significant uncertainty in the results as the contributions from spillover, and to a lesser extent sky emission, are uncertain. For these K- and Q-band observations, the horn apertures are small enough to utilize a liquid nitrogen cooled cold load of known temperature: $T_c = 77$K, allowing a clean separation of receiver temperature from the sky temperature.

Accurate results are critically dependent on the system remaining linear throughout the power range – approximately 10 dB between the cold sky and the hot load. As reported in Memo #85, the power measurement system employed has a non-linearity[1] which becomes notable for input powers exceeding approximately -20dBm. On the other hand, instabilities in the power measurement system itself begin to dominate the radiometric noise for power levels less than approximately -35 dBm. Hence, we set the input power level to ~ -35dBm when on cold sky.

To monitor system gain, we utilized a function generator to switch the internal noise diode on and off with a ten-second period. The noise temperature of the noise diode was itself calibrated against the hot/cold loads.

A brief description follows on the methodology of each session.

3.1 System Temperature, Receiver Temperature, Spillover

A hot and a cold absorber, each of known physical temperature, are alternately placed on top of the feed, and the power from each noted. Presuming linearity and zero offset, the calibration constant and the receiver temperature are derived.

The contributions of atmospheric and ground spillover emission are derived from antenna tips. The antenna is tipped from its vertical position to the lowest elevation of eight degrees, and the power noted at specific elevations. A simple atmosphere and ground emission model is fitted to the data, giving the effective atmospheric emission temperature and opacity. Details of this process are given below.

3.2 Antenna Efficiency and Subreflector Postion

Antenna efficiency measurements require observations of an external source of known flux density, preferably of angular size much smaller than the antenna primary beam to minimize uncertainties in the correction for antenna beam gain. Antenna efficiency measurements are difficult to perform at high frequencies due to fluctuations in system gain and atmospheric emission. Even small clouds will contribute a few Kelvin in added antenna temperature – a value greater than that associated with nearly all extragalactic sources[2]. We thus utilize planets, whose optically thick emission and high disk temperatures provide enough flux at these bands.

The best are the planets Venus, Mars, Jupiter, and Saturn, with disk brightness temperatures of approximately 500, 200, 140, and 100 K, respectively. For all these sources, except Venus at closest approach, the angular size is less than one-half the Q-band beamwidth, thus permitting a simple correction for resolution.

[1] It is believed the origin of this is in the calibration of the E4112E detectors which is appropriate for CW signals, while we are measuring wideband power.

[2] The classic sources Cygnus A, Casseopia A and Virgo A are all too large to be useful at these frequencies.

We utilized Venus when it was near maximum eastern elongation in late October, 2005. At this time, Venus followed the Sun by over 3 hours, allowing the antenna pointing to stabilize, and solar emission to be negligible. At this position, the angular size of Venus was about 25 arcseconds, requiring only minor corrections at K-band, and modest corrections at Q-band for resolution. The flux density from Venus at this time varied from 55 Jy at 18440 MHz to 240 Jy at 48048 MHz, contributing approximately 5 to 10 degrees of antenna temperature at these two bands – sufficient for a good measurement.

Residual antenna pointing errors are always a concern, and as the 'reference pointing' observing mode was not yet available, we observed in a 7 x 7 raster about the nominal position. Hot and cold loads were utilized to calibrate the gain, and the 'slow-switched' noise diode was turned on to monitor gain changes.

Focus errors are also a concern, so to calibrate these, the focus position was checked by moving the subreflector back and forth a few centimeters while tracking Venus.

4 Results

4.1 Calibration

Presuming a linear system with no zero offset, the power measured by the power meter is related to the effective thermodynamic temperature referenced to the input horn by

$$P = GT \tag{1}$$

where G is the system gain, including both the amplifier gain and detection bandwidth. The thermodynamic temperature T comprises two components, the receiver temperature T_r, and the antenna temperature T_a. The receiver temperature accounts for power contributed by the receiver, including the amplifier noise, and any stray emission from the horn and other electronic components. It is expected that the receiver temperature is independent of external factors such as the weather or antenna orientation, and is hence constant. The antenna temperature, T_a, accounts for the power input to the feed, and includes contributions from ground spillover, atmospheric emission, and cosmic radiation, including both the 3K blackbody background and the astronomical source itself. All of these components are considered variable, in the sense that they depend on the direction the antenna is pointing, weather conditions, time of day, etc., and hence are functions of both time and direction.

A measurement of the power received from an optically thick absorber of known physical temperature placed over the feed, plus another measurement from an absorber of a different temperature, are sufficient to determine the two system constants, the gain G and the receiver temperature T_r. Given hot and cold load temperatures T_h and T_c with corresponding power measurements P_h and P_c, we find

$$G = \frac{P_h - P_c}{T_h - T_c} \tag{2}$$

$$T_r = \frac{P_c T_h - P_h T_c}{P_h - P_c}. \tag{3}$$

With these, the antenna temperature T_a of any other source (such as cold sky, or an astronomical emitter) can be determined from the observed power, P_s, as

$$T_a = G^{-1} P_s - T_r \tag{4}$$

$$= \frac{T_c(P_h - P_s) - T_h(P_c - P_s)}{P_h - P_c}. \tag{5}$$

4.2 Receiver and Calibration Temperatures

The receiver temperatures were determined using the method described above. In addition to the receiver temperature, the noise diode temperature, T_{cal}, was also determined. The results are given in Table 1.

Freq MHz	T_{sys} K	T_r K	T_{cal} K
18440	44	23	3.0
23560	47	15	2.6
26120	44	19	1.5
40368	60	23	5.1
43440	70	32	6.4
48048	95	39	6.5

Table 1: The derived cold sky system temperatures, receiver temperatures and noise diode calibration temperatures for EVLA Antenna 14, in LCP. The accuracy is limited by our knowledge of the temperature of the hot load – typically ∼1%.

4.3 Atmospheric Emission and Spillover Temperature

Sky dips were made at all frequencies in order to determine the variation with elevation of the total system temperature. To separate the contribution from spillover from those due to atmospheric emission and cosmic background, a simple atmospheric emission model was adopted, described below.

The total system temperature measured is the sum of an unchanging receiver component, T_r plus an external component, T_a:

$$T_{sys} = T_r + T_a. \tag{6}$$

The receiver component is known from the hot/cold loads, as described above. The antenna temperature contains contributions from the atmosphere and the ground, described here as spillover. The general expression for antenna temperature is:

$$T_a = \frac{\int T_B(\theta,\phi) P(\theta,\phi)\, d\Omega}{\int P(\theta,\phi)\, d\Omega} \tag{7}$$

where $T_B(\theta,\phi)$ is the brighness temperature of the emission, $P(\theta,\phi)$ is the power pattern of the antenna normalized to unity in its forward direction, and the integrals are taken over 4π steradians.

We now assume a two-component emission model, comprising a sky component which enters through the upper 2π steradians, and a ground (spillover) component which enters through the lower 2π steradians. The sky brightness temperature is characterized by

$$T_{sky} = T_{bb} e^{-\tau} + T_{atm}(1 - e^{-\tau}) \tag{8}$$

where $T_{bb} = 2.75$K is the cosmic blackbody background temperature, T_{atm} is the effective radiating temperature of the atmosphere, and $\tau = \tau_0 \sec(z)$ is the atmospheric opacity. The simple $\sec(z)$ model is sufficient here, as effects of earth curvature are appreciable only at elevations below our limit of 8 degrees.

The great majority of the sky emission seen by the antenna enters through or near the main beam, over which the emission is nearly constant, and characterized by Eqn. 8. With this approximation, we can write for the atmospheric contribution to the antenna temperature

$$T_{a,sky} = T_{sky} \frac{\int_{2\pi}^{+} P(\theta,\phi)\, d\Omega}{\int_{4\pi} P(\theta,\phi)\, d\Omega} = T_{sky} \frac{\Omega_{fl}}{\Omega_{4\pi}} \tag{9}$$

where Ω_{fl} is the effective solid angle of the main beam and its nearby sidelobes, and $\Omega_{4\pi}$ is the all-sky integral of the power pattern.

The contribution to the antenna temperature originating from the ground is given by

$$T_{a,sp} = T_{gnd}\frac{\int_{2\pi}^{-} P(\theta,\phi)\,d\Omega}{\int_{4\pi} P(\theta,\phi)\,d\Omega} = T_{gnd}\frac{\Omega_{bl}}{\Omega_{4\pi}} \tag{10}$$

where Ω_{bl} is the effective solid angle of the backlobes of the antenna power pattern. Noting that $\Omega_{fl} + \Omega_{bl} = \Omega_{4\pi}$, we write the antenna temperature as

$$T_a = \epsilon T_{sky} + (1-\epsilon)T_{gnd} \tag{11}$$

where $\epsilon = \Omega_{fl}/\Omega_{4\pi}$ is the forward beam efficiency, describing the fraction of the total power entering the system which originates from the direction of the main beam and its nearby sidelobes, and hence varies with elevation according to the atmospheric emission model given above.

The system temperature data as a function of $\sec(z)$ were then fitted with the following form, resulting from combining equations 8 and 11:

$$T_{sys} = T_r + \epsilon[T_{bb}e^{-\tau_0 \sec z} + T_{atm}(1 - e^{-\tau_0 \sec z})] + (1-\epsilon)T_{gnd}. \tag{12}$$

where T_r is known from the hot/cold load tests. In this expression, there are four parameters which in principle could be determined from the tip curves. However, these curves, except at 48 GHz, deviate only slightly from a linear relation with elevation, so that we expect at most only three unknowns which can be reliably determined. As the air temperature at ground level was well determined (303 K), we fixed the effective ground emission temperature at $T_{gnd} = 305$, and the *effective* atmospheric emission temperature to be 288 K, at K-band, and 276 K at Q-band. The difference reflects the different scale heights between water vapor and oxygen. A least-squares fit for the opacity and main-beam efficiency provided the values shown in red in Figures 2 and 3. The derived parameters are summarized in Table 2.

Freq MHz	τ_0	ϵ	T_r K	T_{sp} K	T_{sky} K	T_{sys} K
18440	.022	0.961	23	12	9	44
23560	.050	0.950	15	15	17	47
26120	.031	0.952	19	15	10	44
40368	.061	0.945	23	17	19	60
43440	.072	0.947	33	16	21	70
48048	.130	0.937	39	19	36	95

Table 2: The derived atmospheric opacity,τ_0, forward efficiency, ϵ, receiver temperature T_r (from the previous section), spillover temperature ($T_{sp} = 305(1-\epsilon)$), antenna temperature T_{sky} due to atmospheric emission (including the 2.7K CMB) at the vertical, for a model where the spillover is not a function of elevation, and total zenith cold-sky system temperature, T_{sys}.

The model fits to the emission at the two upper K-band frequencies are quite good, and provide physically reasonable values for the opacity, corresponding to a precipitable water vapor content (PWV) of 7.7 mm, using the well-known atmospheric model of Liebe (1989). This PWV is remarkably low for the time of year, but a higher and more typical value would require a proportional reduction in the effective atmospheric radiation temperature to a value well below zero centigrade, which is physically unreasonable. The fitted opacity at 18440 MHz is too high compared to that derived from the higher K-band frequencies, presumably because the ground spillover – which has

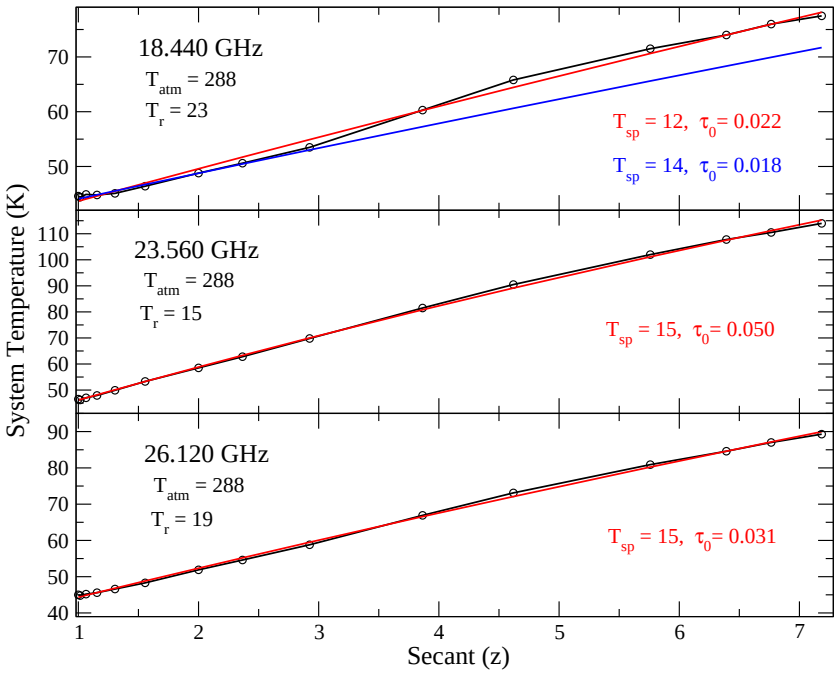

Figure 2: The emission model fits for the K-band data. The effective atmospheric radiating temperature was assumed to be 288K, and the ground temperature taken as 305K. The red lines show the fits for the opacity and spillover contributions shown in red, for a model where the spillover contribution is not a function of elevation. The blue line in the 18440 MHz plot shows the fit for an alternate model, as described in the text.

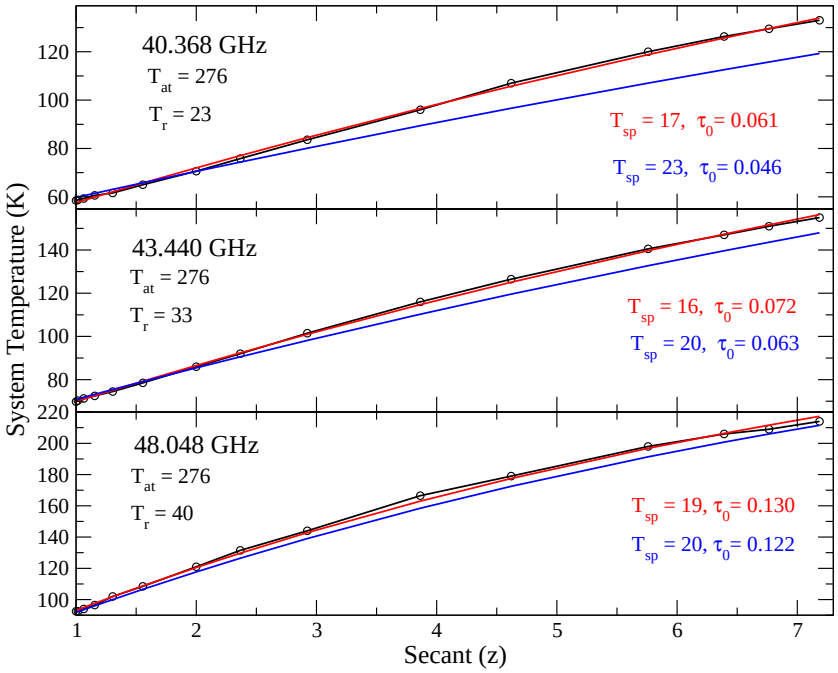

Figure 3: The emission model fits for the Q-band data. The ground temperature was taken as 305K, the effective air temperature 276K. The red lines show the fits for the best-fitting values of opacity and constant spillover. The blue lines show an alternate model where the spillover is allowed to vary with elevation. See the text for details.

roughly the same elevation dependence – is greater at the bottom edge of the band. For this frequency, we have thus adopted an alternate model where the (vertical) opacity is fixed to a value, $\tau_0 = 0.018$ predicted by the Liebe model using a PWV of 7.7mm, and the spillover allowed to vary with elevation. This fit is shown by the blue curve in Fig. 2, with the corresponding parameters given in blue lettering. Note that this fit is very good at the higher elevations (where we might expect the spillover to vary slowly), but departs significantly at low elevations, suggesting an increase in spillover by about 8K over the vertical value of 14K.

A similar procedure was followed for the Q-band fits, as shown in Fig. 3. The red lines show the best fit assuming constant spillover. The blue lines use an opacity calculated using the Liebe model, using PWV = 7.7 mm. As at 18440 MHz, this alternate model requires a larger value of zenith spillover (because of the lower opacity) and an increasing spillover with decreasing elevation, which is particularly large at the bottom end of the band. This is not an unreasonable result, as at the bottom end of the bands, significant horn spillover, beyond the angle subtended by the subreflector, is to be expected, resulting in addition ground pickup at low elevations.

Both models are inadequate to accurately describe the variation in antenna temperature with elevation, although the latter is probably closer to the true situation. To make further progress, full knowledge of angular dependence of the antenna gain function is needed. The benefits of such a study are beyond the scope of this investigation.

5 Subreflector Rotation

Accurate measurements of the optimum subreflector rotation position using an astronomical source are tricky, as rotation of the subreflector offsets the antenna pointing. A simpler method is to observe the total power received as a function of subreflector rotation when observing blank sky. The minimum value will correspond to the optimum illumination of the antenna, which should also be the position of maximum forward gain. Note however that the appropriate quantity to be optimized is the G/T ratio rather than the system temperature, for which the uncorrected correlation coefficient is the desired metric. Future interferometric tests will establish the optimum subreflector position by this means. Nevertheless, we were intrigued by the possibility of using the very simple blank-sky, total-power methodology to determine at least approximately the appropriate subreflector position, so spent a short time investigating this method.

We experimented with this method at both K- and Q-bands, with the results given below. Figure 4 shows the fits using an arbitrary gaussian model at both 23560 MHz and 43340 MHz. The offset between the bands is 20.0 degrees, which compares well with the value of 21.7 degrees determined by interferometry. An error in rotation of one degree moves the antenna beam by 0.46 arcminutes, (approximately half the beamwidth of the antenna at Q-band), so this simple total-power method is sufficient to align the subreflector with fair precision.

6 Efficiency

The K-band observations of Venus were taken in the late afternoon of 26 October, 2005, using the methodology described earlier. Figure 5 shows the data at 23560 MHz.

The Q-band observations were taken in an identical manner in the afternoon of 20 October. For both days, the weather was ideal. Both datasets need correction of focus errors and opacity. For the former, the defocussing was found by tracking Venus while adjusting the focus. This resulted typically in a change in total power of 0.05 to 0.1 dB, corresponding to an increase in antenna temperature of typically 1K. The opacity correction was made using the opacities determined from the atmospheric modelling described earlier.

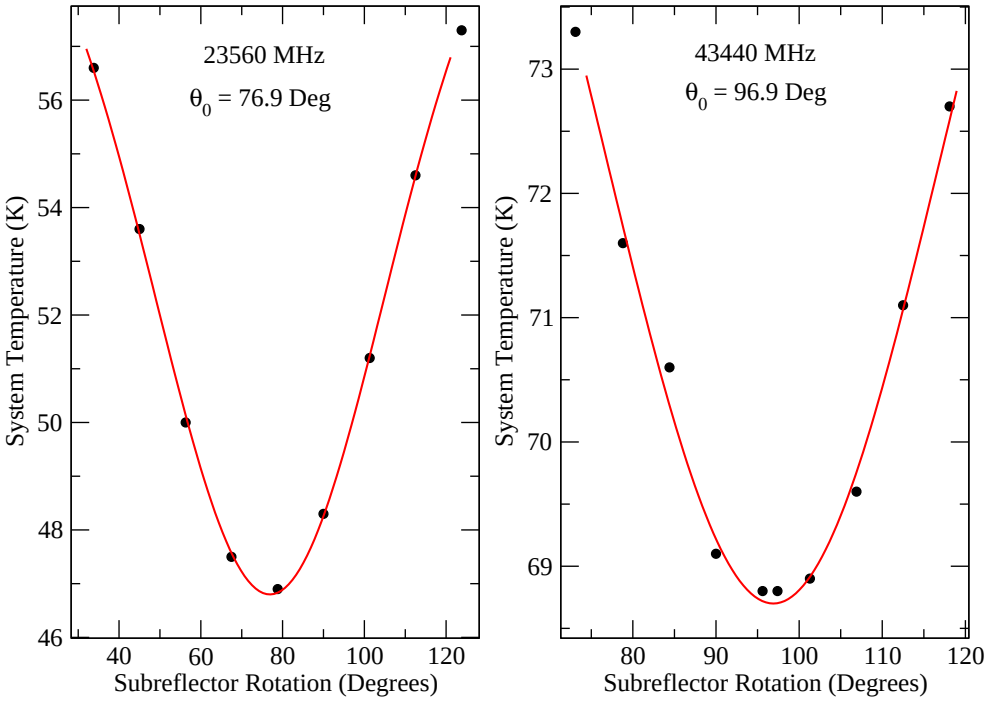

Figure 4: The K-Band (left) and Q-Band (right) system temperature as a function of the subreflector rotation. The black points are the data, and the red lines the fit to an arbitrary gaussian model.

Table 3 gives the results of the system efficiency observations.

Freq MHz	$T_{a,obs}$ K	$T_{a,corr}$ K	S_{Venus} Jy	τ	$S_{V,corr}$ Jy	ϵ
18440	4.7	5.4	55.4	.036	53.4	0.56
23560	5.8	6.9	83.8	.10	75.8	0.51
26120	6.4	7.9	99.8	.063	93.8	0.48
40368	8.1	9.0	183	.044	175	0.29
43440	8.2	9.0	206	.14	178	0.28
48048	7.0	8.7	244	.26	188	0.26

Table 3: The antenna efficiency data. The columns are: (1) Frequency in MHz, (2) Observed antenna temperature due to Venus, (3) Antenna temperature adjusted for focus loss, (4) Venus flux density, adjusted by primary beam dilution, (5) Assumed atmospheric opacity at elevation 30 degrees, (6) Venus flux density, after correction for atmospheric absorption, (7) Derived antenna efficiency (not to be confused with the 'forward efficiency' derived in the previous section).

7 Conclusions

The K-band system easily meets the EVLA requirements: An efficiency of 0.51 and cold-sky zenith system temperature of 61K. At Q-band, the system tempearture meets the EVLA requirements, but the derived efficiency of 0.28 falls somewhat short of the required 0.34. However, accurate efficiency measurements at this highest frequency is fraught with uncertain corrections – source resolution, pointing, and focus/rotation errors may have not been adequately corrected for. In addition, losses due to antenna shape deformations and panel misadjustements are not accounted for. After the

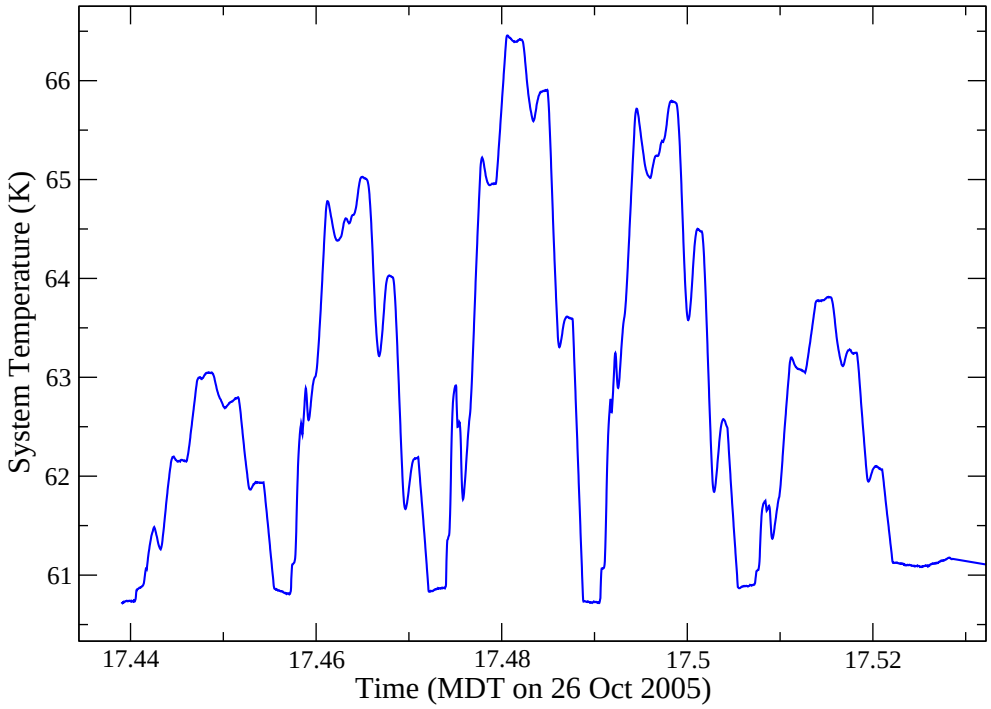

Figure 5: The 7 x 7 raster scans of Venus, taken on 26 Oct., 2005. The source elevation was 30 degrees, accounting for the elevated off-source system temperature.

EVLA outfitting is complete, a round of antenna metrology through holographic measurements will be made, which will very likely result in improved efficiency. We expect the Q-band efficiency requirements will be satisfied after these corrections and improvements are made.

8 Appendix: Absorber Tests

As noted earlier, we performed a number of experiments with different absorbers with the goal of determining which was the most effective as a black body termination. These were motivated by numerous earlier experiments which suggested that the commonly used white-jacketed absorber (whose composition is unknown to us) is not in fact optically thick at microwave wavelengths, with the consequence that the physical temperature of the load could be significantly different than the effective radiation temperature.

The experiments conducted were to place different pairs of absorbers or reflectors on top of the feed, and record the power seen by the system. Differences between different combinations can be used to determine the opacity, and hence the effective temperature, of the various components.

Figure 6 shows one set of experiments with hot loads on the K-band feed. Five different combinations were used: A single piece of Eccosorb CV-3; the 'hot box' used in the AOC laboratory as a hot load, which contains a small piece of CV-3; the result of placing the CV3 on top of the 'hot box'; the white-jacketed absorber alone; and this same absorber with the CV-3 on top.

It is immediately clear that the 'white absorber' is either cooler than the CV3, or it has lower optical depth (or both), since the system temperature is nearly 9K lower than the 'CV3' absorber alone. The rise in system temperature seen when the CV3 is placed on top of the white absorber clearly indicates that differing temperatures are not the primary factor – the white absorber is not optically thick, and lets the horn 'see' some cold background sky emission.

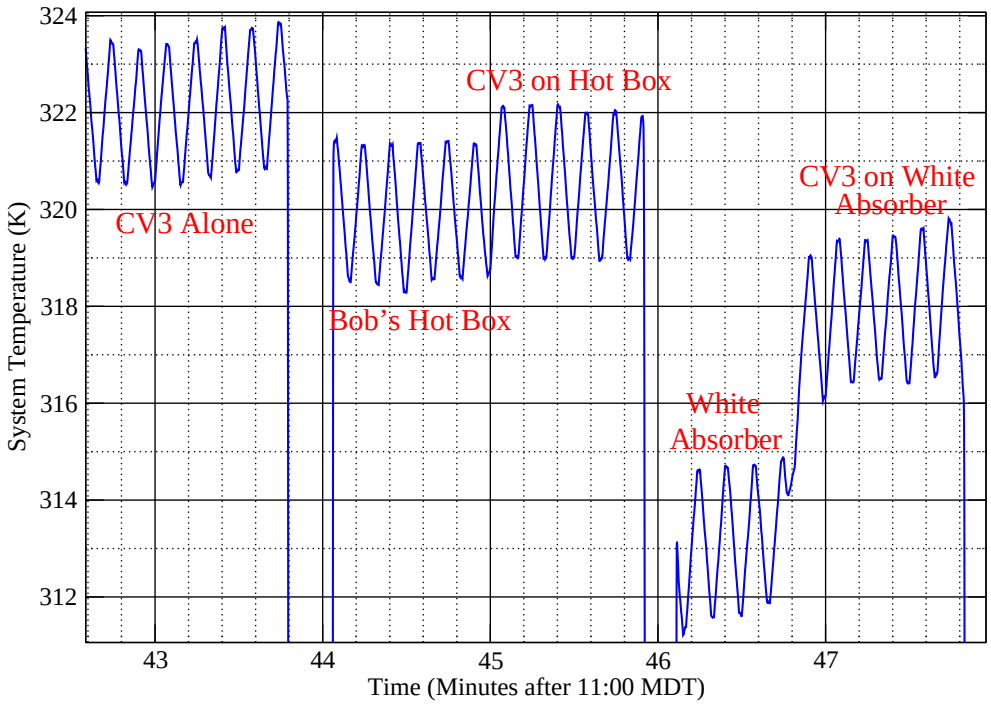

Figure 6: Showing the system temperatures with different combinations of hot loads covering the K-band feed at 18440 MHz. The regular fluctuation in system temperature is due to the 'slow cal' being fired with a 10-second period. The data were sampled at a 10 Hz rate, and have been smoothed with a 4-second boxcar averaging.

It is straightforwards to use these data to compute the optical depths. For a partially transparent absorber of optical depth τ placed on top of the feed, the system temperature will be

$$T_{s1} = T_r + T_{sky}e^{-\tau} + T_w(1 - e^{-\tau}) \tag{13}$$

where T_r is the receiver temperature, and T_w the temperature of the white-jacketed absorber. When we place a layer of 'CV3' on top of the 'white absorber', we get

$$T_{s2} = T_r + T_{cv3}e^{-\tau} + T_w(1 - e^{-\tau}). \tag{14}$$

Differencing, and solving for the optical depth, we find

$$\tau = -\ln\left(\frac{T_{s2} - T_{s1}}{T_{cv3} - T_{sky}}\right) \tag{15}$$

From the plot, we see that the change in system temperature when the CV3 was placed atop the white absorber was 4.7K. The measured temperature of the CV3 was about 305K, while the sky temperature at 18440 MHz (including spillover) was 21K. From these, we find $\tau = -4.12$.

Similarly, the opacity of the 'CV3' can be determined from the pair of measurements labelled 'Bob's Hot Box' and 'CV3 on Hot Box'. In this case, we find $\tau = 6.59$. Alert readers will wonder why the first measurement 'CV3 Alone' provides more power than 'Bob's hot box' – which is also CV3 absorber. The explanation is that the absorber in the 'hot box' is cooler – being placed in a styrofoam box while the 'CV3' is jet black in color and exposed to the sun. Unfortunately, we do not have actual temperatures to confirm this explanation. We also note that the CV3 in the 'hot box' is smaller, and barely covers the horn aperture. Laboratory tests have been done which show

that there is little stray radiation from the laboratory entering the feed so long as the cold box is kept within a few inches of the horn aperture.

Another test (not shown) was to place a metal plate on top of the 'CV3' absorber. The presumption is that this will prevent any leakage of cold sky through the absorber, so that the physical temperature of the absorber will equal the effective radiation temperature. The results show that the power with the plate on is always greater than with it off, as expected, but that the increment is typically 1K – about twice the increment noted when the CV3 was placed on top of the 'white' absorber. We expected the same increment, if the placing of a metal plate is equivalent to putting a truly optically thick absorber on the feed.

A similar round of tests was done at 18440 MHz with the 'Cold Box' – a piece of CV3 immersed in a liquid nitrogen bath, all within a styrofoam box. The results are shown in Fig. 7

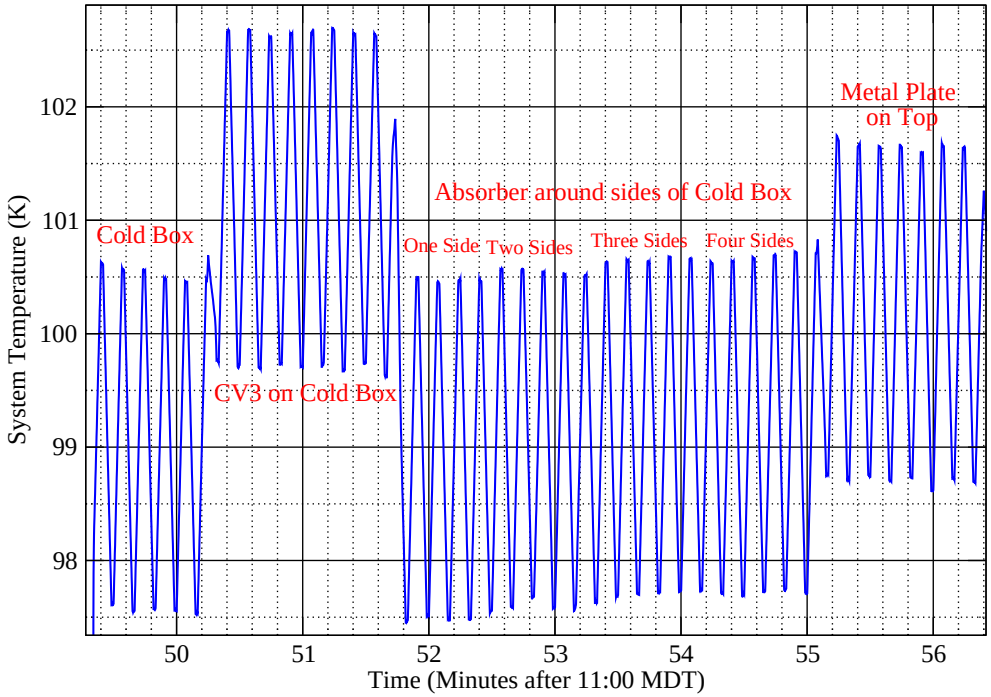

Figure 7: Showing the system temperature with different combinations of cold loads covering the K-band feed.

The first two measurements (on the left side) repeat the CV3 hot load off/on tests described above. The last measurement (far right side) show the effect of placing a reflecting metal plate on the cold load. The three middle experiments show the effect of placing hot loads around the sides of the cold box. These were done to ensure that background emission wasn't coming in 'sideways' into the horn when the cold load was in place. The results clearly show negligible emission leaking in from the sides of the cold load.

We have repeated the analysis to obtain the opacity of the CV3 in the cold box, to find that at the temperature of liquid nitrogen, $\tau = 4.88$. From this, we can calculate the reduction of system temperature when the 'leaky' CV3 is used – it is 0.44K. This is the increase that should be noted when the metal plate is placed on top of the cold load. But in fact, we note an increment of over 1 K – indicating that the metal plate is adding some emission of its own. We conclude that using a metal plate above an imperfect absorber is not a suitable substitute for a truly optically thick absorber. Laboratory measurements show that adding a metal sheet drops the cold load power by

$\sim$0.07 dB, resulting in an improved measurement of the receiver temperature.